Carbonated Hydroxyapatite Coatings with Aligned Crystal Domains

ARTICLE *in* CRYSTAL GROWTH & DESIGN · MAY 2012

Impact Factor: 4.89 · DOI: 10.1021/cg201685x

4 AUTHORS, INCLUDING:

Xue Wei
Greatbatch Medical
6 PUBLICATIONS **28** CITATIONS
SEE PROFILE

Cong Fu
University of Rochester
10 PUBLICATIONS **41** CITATIONS
SEE PROFILE

CRYSTAL GROWTH & DESIGN

Article

pubs.acs.org/crystal

Carbonated Hydroxyapatite Coatings with Aligned Crystal Domains

Xue Wei, Cong Fu, Keith Savino, and Matthew Z. Yates*

Department of Chemical Engineering and the Laboratory for Laser Energetics, University of Rochester, Rochester, New York 14627, United States

ABSTRACT: Carbonated hydroxyapatite coatings were formed on seeded titanium substrates by hydrothermal crystallization in the presence of urea. Decomposition of urea to ammonia and carbon dioxide under hydrothermal conditions was found to have a dramatic effect on crystal morphology and composition of the coatings. Some of the carbon dioxide released by urea decomposition was converted to carbonate ions that substitute for a small fraction of the phosphate groups in the hydroxyapatite crystals. The added urea also suppressed growth of the crystallographic *c*-axis relative to *a*-axis, resulting in a decrease in thickness and an increase in density of the coatings. Repeated hydrothermal growth steps in the presence of urea resulted in dense, highly crystalline coatings with near perfect alignment of the crystallographic *c*-axis normal to the coating surface. The dense coatings can be doped with a variety of other ions, including magnesium, potassium, fluoride, and lanthanum, by addition of appropriate salts in the hydrothermal synthesis. Recent reports have shown that ions move preferentially along the *c*-axis of carbonated apatites at elevated temperature. The morphology of the coatings is therefore ideal for promoting ion transport through the coating to produce electrically polarized bioelectret coatings or ion conducting membranes for electrochemical devices.

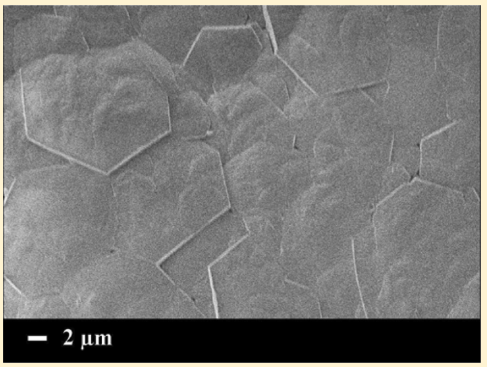

INTRODUCTION

Hydroxyapatite ($Ca_{10}(PO_4)_6(OH)_2$, HAP) is a well-known biomaterial that has also found application in catalysis, gas sensors, and ion exchangers.[1−4] A large family of apatite compounds are formed by partial or complete substitution of the calcium, phosphate, or hydroxyl groups in the HAP crystal framework.[5−9] Calcium sites can be occupied by cations of different valence, such as Na^+, Mg^{2+}, and Y^{3+}. The PO_4^{3-} sites usually accept bivalent anions, such as HPO_4^{2-} and CO_3^{2-}, while both monovalent (F^-) and bivalent anions (CO_3^{2-}) can substitute for hydroxyl groups. The properties of these apatites strongly depend on the crystallinity, chemical composition, and crystal morphology.

Carbonated hydroxyapatite (CO_3HAP) has been shown to have better biocompatibility and osteoconductive properties than HAP because CO_3HAP is more similar in chemical composition to bone tissue.[10,11] The presence of carbonate ions in the apatite lattice is known to improve its mechanical strength and increase solubility.[5,12] The carbonate ions can substitute for either OH^- (A-type) or PO_4^{3-} (B-type) and sometimes both sites can be occupied by carbonate (AB-type). Biological apatites are mainly B-type carbonated apatites with trace amounts of F^-, Cl^-, Na^+, and Mg^{2+}.[13−15] A and B carbonated apatites can be distinguished by their different lattice constants and the different positions of the CO_3^{2-} infrared absorption bands. The characteristic bands of CO_3^{2-} in A-type apatites are observed at 880, 1450, and 1545 cm^{-1} while B-type is characterized by bands at 875, 1410, and 1455 cm^{-1}.[16,17] A-type carbonated apatites are typically obtained by high temperature solid state reactions under a CO_2 atmosphere.[17] Wet chemical precipitation typically produces B-type carbonated apatites, where the pH, reaction temperature, and concentration of reactants affect the properties of the CO_3HAP obtained.[13,16,18]

Our recent research has focused on controlling the microstructure of apatite coatings via hydrothermal crystal growth onto substrates coated with seed crystals.[19−21] In this crystallization process, a HAP seed layer is first deposited electrochemically on a metallic substrate, then multiple hydrothermal crystal growth steps are carried out on the seeded substrate. Under appropriate conditions, dense and well-crystallized apatite coatings are formed in which the *c*-axis of the HAP crystal domains are preferentially oriented normal to the coating surface. Protons are quite mobile along the crystallographic *c*-axis of hydroxyapatite at elevated temperatures,[22] so the microstructure of the coatings is ideal for promoting proton transport. The novel coatings were shown to have proton conductivity orders of magnitude higher than sintered apatite ceramics because the microstructure eliminates grain boundary resistance and minimizes the proton transport path length.[19,23] The high ionic mobility in the coatings potentially allows for easy electrical polarization to create apatite bioelectrets with enhanced osteoconductive properties.[24,25] Electrets are materials with permanent electrical polarization in analogy to magnets that have permanent magnetic polarization. Hydroxyapatite can be polarized at

Received: December 21, 2011
Revised: April 28, 2012
Published: May 10, 2012

   dx.doi.org/10.1021/cg201685x | *Cryst. Growth Des.* 2012, 12, 3474−3480

elevated temperature in an applied electric field because of proton movement, resulting in an stable electret at room temperature or "bioelectret" when used in vivo. Proton conduction in apatites may also allow applications in electrochemical devices such as fuel cells and sensors.

In the present study, urea was studied as a crystal growth modifier during hydrothermal crystallization of hydroxyapatite onto seeded surfaces. Urea slowly decomposes to carbon dioxide and ammonia as the reactant solution is heated. The released NH_3 can gradually increase the reaction solution pH and the released CO_2 dissolves into water as CO_3^{2-}, which can be incorporated into the hydroxyapatite crystal structure to form CO_3HAP.[13,18,26,27] Urea therefore has a profound effect on crystal growth and morphology by regulating solution pH and crystal composition. By adding urea during hydrothermal crystal growth onto seeded substrates, dense CO_3HAP coatings can be obtained with *c*-axis alignment normal to the substrate. The novel CO_3HAP morphology reported here may prove advantageous in application in biomedical implants, bioelectrets, and electrochemical devices.[28−30]

EXPERIMENTAL SECTION

Materials. NaCl (≥99.0%), tris(hydroxymethyl)-aminomethane (99.8+%), $Ca(NO_3)_2{\cdot}4H_2O$ (99.0%), $Mg(NO_3)_2{\cdot}6H_2O$ (99%), $La(NO_3)_3{\cdot}6H_2O$ (99.999%), urea (99.5%), NH_4F (98+%), and disodium ethylenediaminetetraacetate dihydrate ($Na_2EDTA{\cdot}2H_2O$) (99.0−101.0%) were all from Sigma-Aldrich (Saint Louis, MO, U.S.A.). $(NH_4)_2HPO_4$ (>99.0%) was from EMD Millipore (Billerica, MA, U.S.A.). KNO_3 (99%), was from EM Science (Cherry Hill, NJ, U.S.A.). K_2HPO_4 (99.99%), $CaCl_2{\cdot}2H_2O$ (99+%). hydrochloric acid (37%), and ammonium hydroxide (28.0−30.0%, analytical pure) were from Mallinckrodt Chemicals (Phillipsburg, NJ, U.S.A.). Titanium (Ti) (99.7%, 0.89 mm thick, grade 2) plate and platinum (Pt) (99.9%, 0.127 mm thick) foils were from Alfa Aesar (Ward Hill, MA, U.S.A.). The salts, particularly nitrates, are very hygroscopic and should not be exposed to humid air.

Sample Preparation and Characterization. The hydroxyapatite seed layer was deposited on titanium following a previously reported electrochemical method.[19,21] Ti plates (12.5 by 12.5 by 0.89 mm) were polished with SiC sand paper (1500 grit) and washed with an industrial detergent solution, then cleaned ultrasonically for 30 min in aqueous detergent solution followed by 30 min in ethanol/acetone (volume ratio = 50/50). The cleaned Ti plate was used as the cathode for electrochemical deposition of HAP and the anode was a platinum plate (25 by 25 by 0.127 mm). The anode and cathode were maintained parallel to one another at a fixed distance of separation of 10 mm using a custom Teflon holder. The electrodes were connected to a power supply (Instek, GPS-3030D) using platinum wire for the anode and silver wire for the cathode. The electrodes were then submerged in an aqueous electrolyte solution consisting of 1.38×10^{-1} mol/L NaCl, 5×10^{-2} mol/L tris(hydroxymethyl)-aminomethane buffer, 1.3×10^{-3} mol/L $CaCl_2$, and 8.4×10^{-4} mol/L K_2HPO_4 that was adjusted to pH 7.2 at room temperature using 37% hydrochloric acid. The electrolyte solution was maintained at ∼95 °C using an oil bath. Both the electrolyte solution and oil-bath were stirred continuously at a rate of 200 rpm using magnetic stir bars. Electrochemical deposition was carried out for 5 min with a constant current density of 12.5 mA/cm^2 based on the area of anode. During deposition, the applied voltage was between 3.3 to 3.7 V. After electrochemical deposition, the titanium seeded with HAP crystals was taken out of the electrolyte solution, rinsed with deionized water several times, and dried in air.

For a typical hydrothermal crystallization, Na_2EDTA (4.28 g) was first completely dissolved into 0.1 L deionized water, then $Ca(NO_3)_2{\cdot}4H_2O$ (2.36 g), $(NH_4)_2HPO_4$ (0.79 g), and urea (1.2 g) were successively added and the solution was stirred for 30 min to saturate the Ca-EDTA complex. Ion substitution was carried out in select experiments by adding potassium nitrate, magnesium nitrate, lanthanum nitrate, or ammonium fluoride to form a concentration of 0.01 mol/L. The solution was then adjusted to pH 10.0 with ammonium hydroxide. Then 3×10^{-2} L of fresh solution was used for the hydrothermal reaction carried out in a Teflon-lined pressure vessel (Parr Instruments model 4744). The seeded substrate was fixed onto a Teflon plate by titanium wire and submerged in the solution in the pressure vessel. The length of the Teflon plate holding the sample was slightly longer than the inner diameter of the pressure vessel, so that the sample was resting at an angle of ∼45 degrees relative to the bottom of the vessel with seed layer facing down. Then, the pressure vessel was sealed and placed in a preheated oven (YAMATO DX 300). The hydrothermal reaction was carried out at 200 °C for 15 h in air. This process was repeated for 4 times. After the reaction, the vessel was cooled to room temperature in air. The sample was taken out, rinsed with deionized water several times, and dried in air.

The coating morphology was examined using a field-emission source scanning electron microscope (FESEM, Zeiss-Leo DSM982, Carl Zeiss SMT GmbH, Oberkochen, Germany) equipped with an energy dispersive X-ray spectrometer (EDX Phoenix). The crystal structure was determined by X-ray diffraction (XRD) (PW3020, Philips, Almelo, Netherlands) with Cu Kα radiation (λ = 1.5418 Å) in the 2θ range from 20° to 60°. The Fourier transform infrared (FTIR) spectra were obtained using a spectrophotometer (FTIR-8400S, Shimadzu, Kyoto, Japan) in the range of 500−2000 cm^{-1}. The chemical composition of the coating was analyzed by elemental analyzer (CE-440, Exeter Analytical Inc., North Chelmsford, MA, U.S.A.) and electron-probe microanalyzer (JXA-8900, JEOL, Tokyo, Japan).

RESULTS AND DISCUSSION

During electrochemical deposition, the titanium substrate acts as the cathode as a direct current is applied through the HAP synthesis solution. Electrolysis of water causes an increase in pH near the surface of the cathode and an accumulation of calcium ions by electrostatic attraction. As described by Ban and Maruno, the cathodic potential causes a flux of both cations and anions near the cathode surface.[31] The changes in pH and ion concentration caused by the applied current results in a local supersaturation of HAP near the cathode, so that crystals grow selectively on the titanium surface.[31−33] The electrochemical reaction time was purposely kept short to avoid dislodging HAP crystals by hydrogen gas bubbles that evolve from the titanium surface through the electrolysis of water that is required for crystal growth. Over longer reaction times, the evolving gas bubbles cause the HAP coating to become nonuniform.[20] It was found that an electrochemical reaction time of 5 min resulted in a uniform HAP seed layer over the entire titanium surface. As shown in Figure 1a and b, the resulting HAP seed crystals have a needle-like morphology with a length of 1−2 μm and 100−200 nm width. The morphology is consistent with other studies of electrochemical crystallization of HAP in which the long axis of the rod-shaped crystals is associated with the crystallographic *c*-axis.[32,33] Figure 1c shows the X-ray diffraction pattern of the seed layer. All diffraction peaks from the seed layer correspond to HAP, and no secondary phases were observed. The relative intensity of the (002) to (300) planes indicates some preferred orientation of the *c*-axis normal to the metal substrate.

Additional growth onto the seeded substrate was then carried out using hydrothermal crystallization mediated by the cation chelating agent EDTA. Upon heating, the calcium-EDTA chelate breaks down to release free calcium ions that react with the phosphate to form HAP. The complexation of calcium with EDTA controls supersaturation to limit homogeneous nucleation and growth of HAP from solution.[34,35] As a result,

dx.doi.org/10.1021/cg201685x | Cryst. Growth Des. 2012, 12, 3474−3480

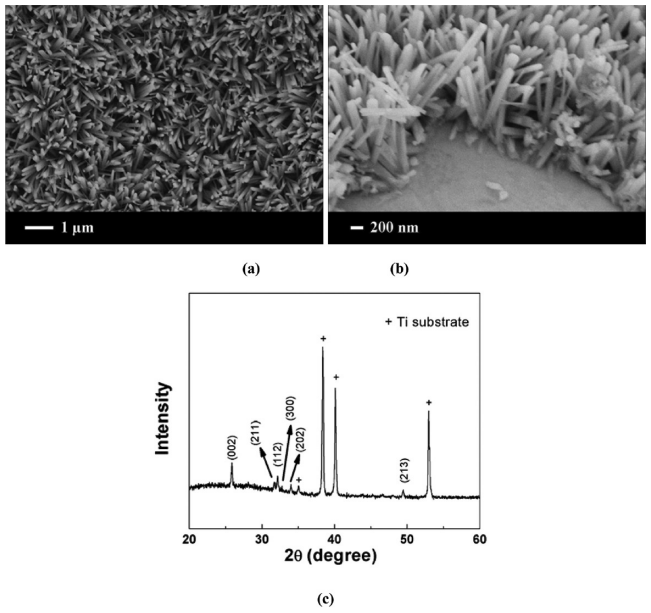

Figure 1. SEM images (a and b) and XRD pattern (c) of HAP seed layer on titanium prepared by electrochemical deposition at 12.5 mA/cm^2 current density at 95 °C for 5 min: (a) top-view and (b) side-view.

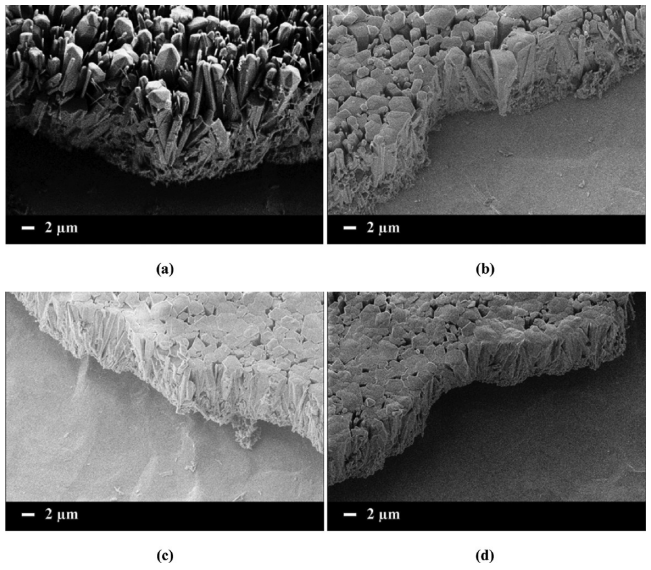

Figure 2. Side-view SEM images of HAP and CO_3HAP coatings as a function of starting urea concentration in the hydrothermal process: (a) No urea, (b) [urea] = 0.1 M, (c) [urea] = 0.2 M, and (d) [urea] = 0.3 M.

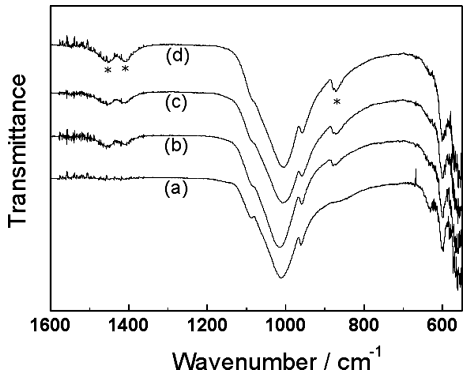

Figure 3. FTIR spectra of (a) HAP coating without urea, and CO_3HAP coatings formed with urea concentrations of (b) 0.1, (c) 0.2, and (d) 0.3 M. The carbonate peaks are marked with asterisks on d.

EDTA promotes HAP crystal growth onto seeded substrates, as previously reported.[19,21] Unlike previous studies, urea was also added to the hydrothermal synthesis starting solution. As the solution is heated, the urea decomposes to ammonia and carbon dioxide. The carbon dioxide provides carbonate ions. Some of the carbonate ions can be incorporated into HAP to form carbonated apatite crystals.

The effect of urea on the hydrothermal crystal growth onto the seeded substrate was investigated. Crystallization was carried out for 15 h at 200 °C with a starting pH of 10. The resulting coatings were purposely fractured using a metal blade to allow observation of the coating thickness and surface morphology using SEM. The results are shown in Figure 2. Hexagonal facets of the crystals are clearly visible on the upper surface, indicating *c*-axis orientation normal to the substrate. Without urea, the coating thickness was ∼15 μm and many gaps between crystals were observed. With 0.1 M urea, the coating thickness was reduced to ∼9 μm. The coating thickness was further reduced to ∼6 μm when the urea concentration was increased to 0.2 M. Additional increase in urea concentration to 0.3 M did not result in any discernible difference in morphology compared to coatings formed with 0.2 M urea. The SEM results show that, as urea concentration is raised, the coatings become thinner with less open space between crystals.

Carbonate incorporation into the coatings was confirmed with FTIR spectroscopy, as shown in Figure 3. The absorption bands at 958, 1005, and 1088 cm^{-1} are due to the PO_4^{3-} group. The librational vibration of OH^- groups appears at 631 cm^{-1}. The sample prepared without urea does not contain significant amounts of carbonate since no obvious absorption peak was found in the range of 1400−1600 cm^{-1}. It is possible that a slight amount of carbonate comes from CO_2 in the air headspace sealed in the reactor. For the samples prepared in the presence of urea, additional peaks for the CO_3^{2-} group appear at 872, 1408, and 1453 cm^{-1}, indicating that the as-prepared coatings are mainly B-type carbonated HAP. The FTIR spectra also show that the absorption bands of PO_4^{3-} at 1088 weaken, while those of CO_3^{2-} strengthen with increasing concentration of urea, implying that the level of carbonate substitution in the HAP lattice increases.

For all samples shown in Figure 2, the initial pH was 10 and after the hydrothermal reaction it was ∼9.6 on average in repeated experiments. Therefore, we infer that the urea induced morphology change is a result of the CO_3^{2-} incorporation into the hydroxyapatite crystals rather than a significant change in pH from the ammonia released by urea decomposition. Hydroxyapatite has two types of crystal planes; a positively charged calcium-rich *a*-plane and a negatively charged hydroxyl and phosphate rich *c*-plane.[36] The FTIR analysis shows that carbonate ions mainly occupy the phosphate sites. As a result, the CO_3^{2-} will be found on the *c*-plane surfaces along with phosphate and hydroxyl groups. The morphological changes observed by SEM indicate the *c*-planes become larger with increasing urea concentration, while the length of the *c*-axis is reduced. Carbonate substitution is known to decrease the aspect ratio of hydroxyapatite *c*-axis/*a*-axis in some solution based synthesis methods.[37] It is possible that free CO_3^{2-} ions in solution promote *a*-axis growth at the expense of *c*-axis growth due to the strong interaction between CO_3^{2-} and the positively

dx.doi.org/10.1021/cg201685x | *Cryst. Growth Des.* 2012, 12, 3474−3480

charged *a*-planes. Therefore, CO_3^{2-} substitution gives rise to a thinner, more dense surface coverage with larger crystal domains in the plane of the coating.

The starting pH had a significant effect on the morphology of CO_3HAP coatings grown onto the seeded substrates. At higher pH, the coatings were thinner and more dense as shown in Figure 4. The coatings produced with starting pH of 7 and 9

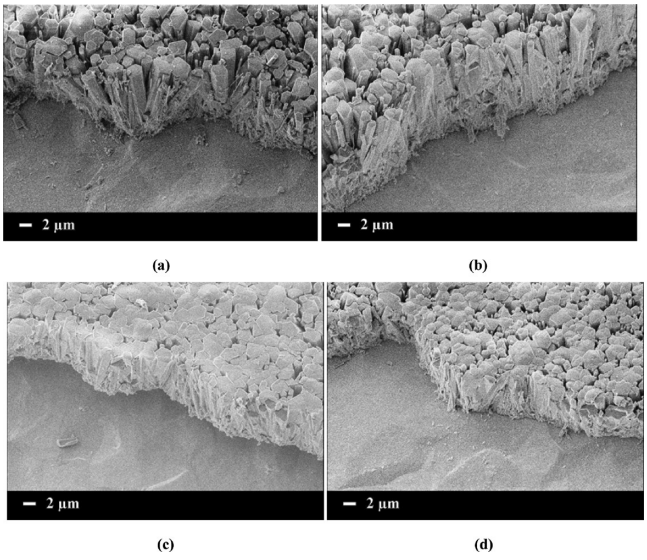

Figure 4. Side-view SEM images of CO_3HAP coatings as a function of starting pH in the hydrothermal process: (a) pH = 7, (b) pH = 9, (c) pH = 10, and (d) pH = 10.5.

had a similar morphology with thickness of ~12 μm and significant open space between the crystals. The thickness of the coatings was reduced to ~7 μm when the pH was increased from 9 to 10. The coating density appeared to increase when the pH was raised from 9 to 10 since less space was observed between crystals in both top view and side view images. Further increase of the pH to 10.5 resulted in slightly lower coating thickness of ~6 μm, with a morphology appearing similar to that produced at pH 10. The observed changes in morphology and thickness with pH are likely due to the incorporation of CO_3^{2-} into the HAP lattice. It has been reported that the level of CO_3^{2-} substitution into the HAP lattice is pH dependent with the maximum level occurring around pH 10.[15] Since CO_3^{2-} incorporation effectively promotes crystal growth along the *a*-axis relative to the *c*-axis, thinner and more dense coatings are consistent with a higher level of CO_3^{2-} substitution.

Temperature is also a critical factor influencing the crystal morphology, coating thickness, and crystal composition since it controls the rates of decomposition of both urea to release CO_3^{2-} and Ca-EDTA to release Ca^{2+}. Upon heating the solution, the slow release of these ions causes the solution to become supersaturated, and the seed HAP crystals start to grow with carbonate substitution. Figure 5 shows the side-view morphology of CO_3HAP coatings deposited after 15 h under different reaction temperatures at pH 10. As shown in Figure 5a, the crystals obtained at 150 °C still have needle-like morphology, similar to those of the HAP seed layer. This indicates 150 °C is too low for the decomposition of the calcium complex, and little or no crystal growth occurred. The crystals size increased remarkably as the temperature was increased to 180 °C, as shown in Figure 5b. The coating

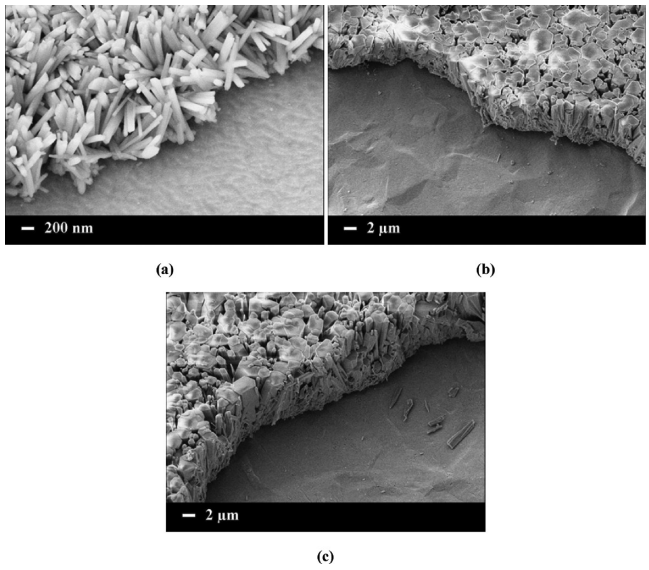

Figure 5. Side-view SEM images of CO_3HAP coatings as a function of reaction temperature in the hydrothermal process: (a) 150, (b) 180, and (c) 220 °C.

obtained at 180 °C, contains well-developed hexagonal crystals with a width up to 2 μm and a length of ~5 μm. Coatings produced at 200 °C (Figure 4c) and 220 °C (Figure 5c) show a similar morphology of well-developed hexagonal crystals. The length of the *a*-axis did not change significantly from 180 to 220 °C. The increase in crystal size above 180 °C is primarily due to increase in growth along the *c*-axis, possibly due to the higher rate of decomposition of the calcium complex during crystal growth.

The effect of reaction time was also investigated for fixed initial pH and temperature of 10.0 and 200 °C, respectively. Figure 6 reveals that the coating has already grown to its

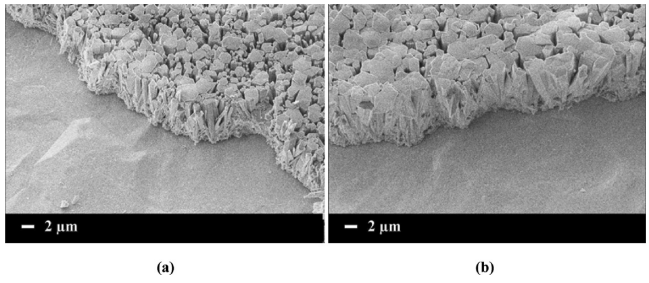

Figure 6. SEM images of CO_3HAP coatings as a function of reaction time in the hydrothermal process: (a) 5 h and (b) 10 h.

maximum thickness after 5 h. As the reaction time is increased from 5 to 10 h, the CO_3HAP coating density increases, based on SEM observation, as the crystals grow notably wider but have very little growth in length. A further increase of the reaction time from 10 to 15 h does not result in an obvious increase in crystal size (shown in Figure 4c). The results suggest that the reaction reaches completion after ~10 h. It is notable that the crystal growth is initially fast in the *c*-axis direction but then becomes faster in the *a*-axis direction before the reaction is completed. For normal hydroxyapatite, the *c*-axis is always fastest growing during hydrothermal synthesis unless a surfactant is added to modify crystal growth.[19] Since CO_3^{2-} substitution promotes *a*-axis growth,[37] the study suggests that

dx.doi.org/10.1021/cg201685x | *Cryst. Growth Des.* 2012, 12, 3474–3480

at 200 °C there is a delay in the effect of CO_3^{2-} substitution on the rate of *a*-axis growth relative to the *c*-axis. The delay may be due to differences in the kinetics of release of calcium versus carbonate ions.

It was found that repeated hydrothermal crystal growth steps enable the formation of dense CO_3HAP, as shown in Figure 7.

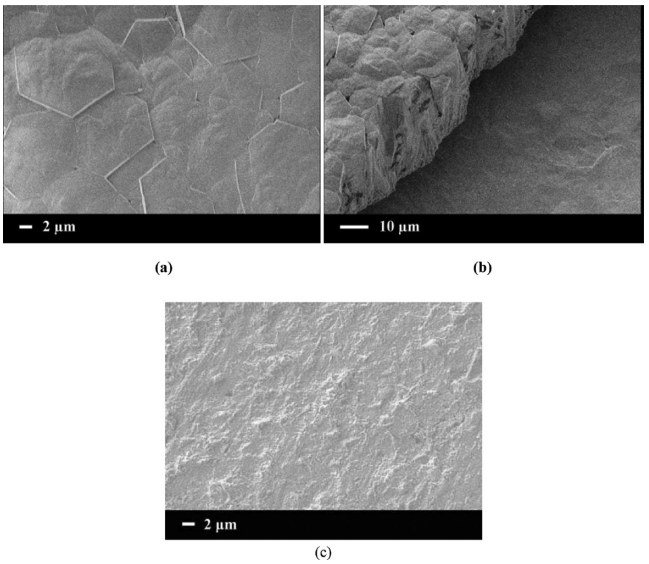

Figure 7. Dense CO_3HAP coatings prepared by four repeated hydrothermal reactions: (a) top-view image (b) side-view image (c) underside image.

The SEM images in Figure 7a and b show that all crystal domains grow together to form a dense coating with a thickness of approximately 25 μm, after four 10 h crystallization steps. Hexagonal facets visible on the upper surface of the coating show that the crystal domains maintain the preferred orientation of the *c*-axis normal to the substrate. The process resulted in complete and uniform coating of the Ti substrate. An adhesion test (ASTM D3359) was conducted on dense CO_3HAP coating. A razor blade was used to make an X-cut through the coating to the substrate. Then an adhesive tape (Elcometer 99) was applied and removed. The coating's adhesive strength is qualitatively measured based on the percent of coating removed by the tape. It was found that cutting the film with the razor caused brittle fracture and flaking of most of the coating in the X-cut area. Figure 7c shows the dense and rough underside of the coating removed by the blade. Of the coating remaining after cutting, very little was removed by the adhesive tape. When adhesive tape was applied to the dense coating without cutting, none of the coating was lost upon removal of the tape. The results show that the CO_3HAP coating adheres strongly to the metal, but is susceptible to brittle fracture. Elemental analysis of dense CO_3HAP coatings showed the composition in weight percent was 37.4% Ca, 17.5% P, 1.2% C, and 1.1% Na. The Ca/P molar ratio is therefore 1.65. The carbon is from carbonate substituting for phosphate groups in the crystal. A better indication of the calcium deficiency relative to stoichiometric composition is obtained by considering the molar ratio of Ca/(P + C), which is 1.41. The measured sodium is from Na_2EDTA used in the hydrothermal reaction.

Various salts were added to the hydrothermal reaction in order to introduce ions known to substitute for calcium and hydroxyl ions in the apatite coatings. Potassium nitrate, magnesium nitrate, lanthanum nitrate, or ammonium fluoride were added to produce coatings shown in rows 1−4, respectively, in Figure 8. Figure 8a(1−4) show the morphology after a single 15 h hydrothermal step without urea. In each case, long rod-shaped crystals are produced, indicating that none of the added salts enhance *a*-axis growth relative to the *c*-axis. In comparison, Figure 8b(1−4) show the morphology after a single 15 h hydrothermal step at the same conditions used in Figure 8a(1−4) except 0.2 mol/L urea was added. In every case, when urea is added the length of the crystallographic *a*-axis is enhanced relative to the *c*-axis, resulting in a more dense coating. After four repeated 10 h crystallization steps, the thickness and density of the coatings increased, as shown in Figures 8c(1−4). Electron probe microanalysis was used to confirm that F, La, Mg, and K ions are incorporated into the HAP crystals. For each of the ions, the synthesis solution had a molar ratio of ion:Ca of 1:10. The cation:Ca molar ratio in the final coatings were measured to be 0.52:10, 0.10:10, 0.02:10, and 0.002:10 for F, Mg, La, and K, respectively. Therefore, 52% of the added fluoride was incorporated into the coatings, while only 0.2% of the added potassium was incorporated. The results in Figure 8 demonstrate that hydrothermal crystallization in the presence of urea is a robust method for forming dense apatite coatings. The fact that crystal morphology is insensitive to the added salts suggests that the crystals may be doped in a controlled manner using urea to maintain the coating morphology and added salts to adjust coating composition.

X-ray diffraction patterns of the dense coatings are shown in Figure 9. The intensity of the (002) and (004) diffraction peaks is enhanced relative to all other peaks when the *c*-axis is preferentially oriented normal to the substrate. The only diffraction peaks visible in Figure 9 are those corresponding to the (002) and (004) planes, indicating near perfect orientation of crystal domains normal to the substrate for all dense coatings synthesized. Figure 10 shows the X-ray diffraction pattern of the CO_3HAP coating after removing it from the titanium substrate by scraping with a blade and crushing it into a powder. No secondary crystal phases are evident in the diffraction pattern in Figure 10. The relative peak intensities are significantly different in Figure 10 than in Figure 9 due to the random crystal orientation in the powder sample. Figure 10 also confirms that the peak intensities in Figure 9 are a result of crystal orientation and not other crystal phases.

The growth mechanism is analogous to that of zeolite and molecular sieve membranes produced by repeated hydrothermal crystallization onto seeded substrates.[38−40] During repeated hydrothermal growth steps, crystals oriented with the fastest growing axis normal to the substrate grow larger at the expense of crystal oriented in other directions.[38] The evolution of crystal orientation during growth on seeded substrates was first explained by van der Drift as an "evolutionary selection" process.[41] For hydroxyapatite, the *c*-axis is typically the fastest growing.[42] As a result, it is expected that *c*-axis orientation normal to the substrate will become dominant upon repeated hydrothermal growth steps.

■ CONCLUSIONS

Urea plays two simultaneous roles during hydrothermal crystal growth of hydroxyapatite onto a seeded substrate. First, high temperature decomposition of urea releases carbonate ions that substitute for a fraction of the phosphate groups in the growing crystals. Second, the added urea suppresses *c*-axis growth

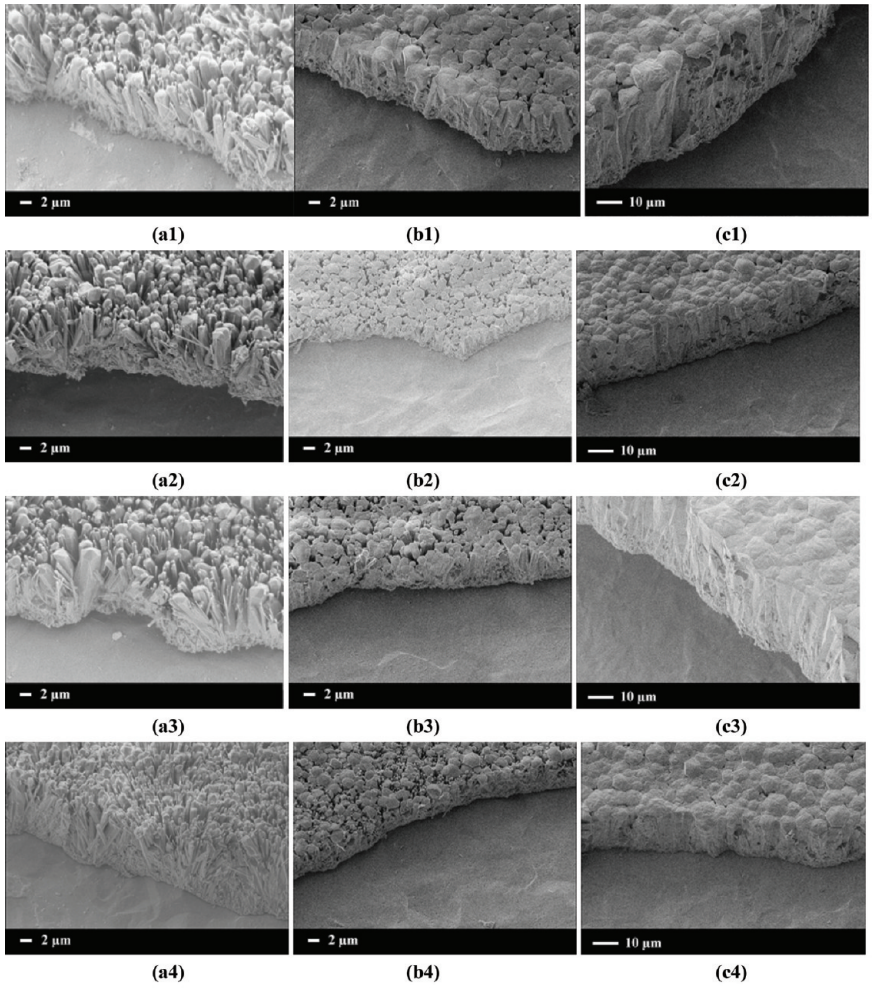

Figure 8. Side-view SEM images of apatite coatings prepared by electrochemical/hydrothermal method at 200 °C and pH = 10. Rows 1−4 correspond to coatings obtained with added potassium, magnesium, lanthanum, and fluoride, respectively. Column "a" is the coating obtained without urea after a single hydrothermal crystallization for 15 h. Column "b" is the coating obtained after a single hydrothermal crystallization for 15 h with 0.2 M urea added. Column "c" is the dense coating obtained after 4 repeated 10 h crystallization steps with 0.2 M urea added.

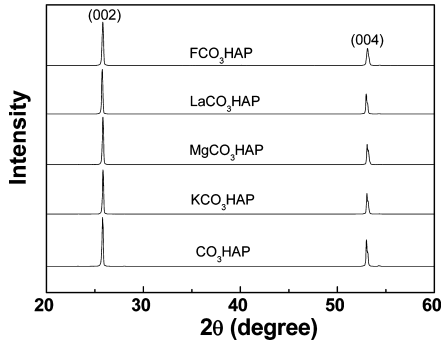

Figure 9. XRD pattern of dense carbonated apatite coatings on Ti substrates.

relative to *a*-axis, resulting in thinner and denser coatings. Dense carbonated apatite coatings with very good alignment of the *c*-axis normal to the substrate can be formed using urea as a crystal growth modifier. The crystal alignment results in the expression of negatively charged hydroxyl and phosphate rich c-planes at the surface. Further work is needed to investigate the utility of these novel hydroxyapatite coatings. The unique surface free energy and surface chemistry may play a role in osteoconduction in orthopedic applications. The *c*-axis is also known to conduct ions at high temperature, making the coatings potential candidates for use as bioelectrets or membranes in electrochemical applications.

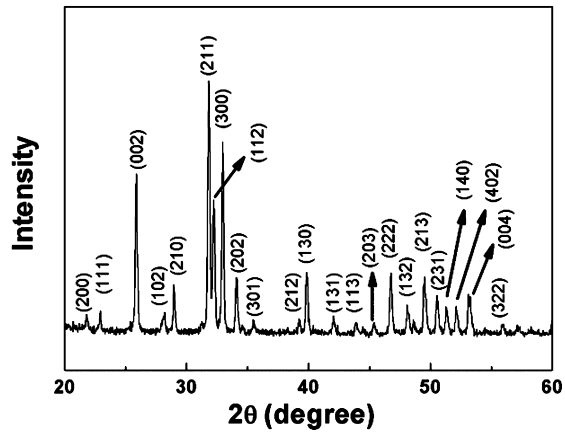

Figure 10. XRD pattern of dense carbonated apatite coating after removing from substrate and grinding to a powder. All diffraction peaks are consistent with hydroxyapatite (JCPDS card No. 86-0740).

dx.doi.org/10.1021/cg201685x | *Cryst. Growth Des.* 2012, 12, 3474−3480

AUTHOR INFORMATION

Corresponding Author

*E-mail: myates@che.rochester.edu. Tel: +1 585 273 2335. Fax: +1 585 273 1348.

Notes

The authors declare no competing financial interest.

ACKNOWLEDGMENTS

We acknowledge NSF (CMMI-0856128), the DOE through the Laboratory for Laser Energetics (DE-FC03-92SF19460), and the University of Rochester for supporting this research.

REFERENCES

(1) Kibby, C. L.; Hall, W. K. *J. Catal.* **1973**, *31*, 65−73.
(2) Nagai, M.; Saeki, T.; Nishino, T. *J. Am. Ceram. Soc.* **1990**, *73*, 1456−1460.
(3) Suzuki, T.; Hatsushika, T.; Miyake, M. *J. Chem. Soc., Faraday Trans. I* **1982**, *78*, 3605−3611.
(4) Yamashita, K.; Kitagaki, K.; Umegaki, T. *J. Am. Ceram. Soc.* **1995**, *78*, 1191−1197.
(5) Boanini, E.; Gazzano, M.; Bigi, A. *Acta Biomater.* **2010**, *6*, 1882−1894.
(6) Cacciotti, I.; Bianco, A.; Lombardi, M.; Montanaro, L. *J. Eur. Ceram. Soc.* **2009**, *29*, 2969−2978.
(7) Feki, H. E.; Savariault, J. M.; Salah, A. B.; Jemal, M. *Solid State Sci.* **2000**, *2*, 577−586.
(8) Matsunaga, K.; Inamori, H.; Murata, H. *Phys. Rev. B* **2008**, *78*, 8.
(9) Narasaraju, T. S. B.; Phebe, D. E. *J. Mater. Sci.* **1996**, *31*, 1−21.
(10) Krajewski, A.; Mazzocchi, M.; Buldini, P. L.; Ravaglioli, A.; Tinti, A.; Taddei, P.; Fagnano, C. *J. Mol. Struct.* **2005**, *744*−*747*, 221−228.
(11) Muller, F. A.; Muller, L.; Caillard, D.; Conforto, E. *J. Cryst. Growth* **2007**, *304*, 464−471.
(12) Pan, H.; Darvell, B. W. *Cryst. Growth Des.* **2010**, *10*, 845−850.
(13) Wu, Y.-S.; Lee, Y.-H.; Chang, H.-C. *Mater. Sci. Eng., C* **2009**, *29*, 237−241.
(14) Xiao, X.; Liu, R.; Gao, Y. *Mater. Sci. Technol.* **2008**, *24*, 1199−1203.
(15) Yusufoglu, Y.; Akinc, M. *J. Am. Ceram. Soc.* **2008**, *91* (1), 77−82.
(16) Aizawa, M.; Ueno, H.; Itatani, K.; Okada, I. *J. Eur. Ceram. Soc.* **2006**, *26*, 501−507.
(17) Fleet, M. E.; Liu, X. *J. Solid State Chem.* **2003**, *174*, 412−417.
(18) Zhang, Y.; Lu, J.; Wang, J.; Yang, S.; Chen, Y. *J. Cryst. Growth* **2009**, *311*, 4740−4746.
(19) Liu, D. X.; Savino, K.; Yates, M. Z. *Adv. Funct. Mater.* **2009**, *19*, 3941−3947.
(20) Liu, D.; Savino, K.; Yates, M. Z. *Surf. Coat. Technol.* **2011**, *205*, 3975−3986.
(21) Wei, X.; Fu, C.; Savino, K.; Yates, M. Z. *Cryst. Growth Des.* **2012**, *12*, 217−223.
(22) Nakamura, S.; Takeda, H.; Yamashita, K. *J. Appl. Phys.* **2001**, *89*, 5386−5392.
(23) Wei, X.; Yates, M. Z. *Chem. Mater.* **2012**.
(24) Teng, N. C.; Nakamura, S.; Takagi, Y.; Yamashita, Y.; Ohgaki, M.; Yamashita, K. *J. Dent. Res.* **2001**, *80*, 1925−1929.
(25) Nakamura, M.; Nagai, A.; Okura, T.; Sekijima, Y.; Hentunen, T.; Yamashita, K. *J. Ceram. Soc. Jpn.* **2010**, *118*, 474−478.
(26) Lin, K.; Chang, J.; Zhu, Y.; Wu, W.; Cheng, G.; Zeng, Y.; Ruan, M. *Cryst. Growth Des.* **2008**, *9*, 177−181.
(27) Neira, I. S.; Kolen'ko, Y. V.; Lebedev, O. I.; Van Tendeloo, G.; Gupta, H. S.; Guitian, F.; Yoshimura, M. *Cryst. Growth Des.* **2009**, *9*, 466−474.
(28) Bouhaouss, A.; Bensaoud, A.; Laghzizil, A.; Ferhat, M. *Int. J. Inorg. Mater.* **2001**, *3*, 437−441.
(29) Gittings, J. P.; Bowen, C. R.; Dent, A. C. E.; Turner, I. G.; Baxter, F. R.; Chaudhuri, J. B. *Acta Biomater.* **2009**, *5*, 743−754.
(30) Tanaka, Y.; Kikuchi, M.; Tanaka, K.; Hashimoto, K.; Hojo, J.; Nakamura, M.; Nagai, A.; Sugiyama, T.; Munakata, F.; Yamashita, K. *J. Am. Ceram. Soc.* **2010**, *93*, 3577−3579.
(31) Ban, S.; Maruno, S. *Jpn. J. Appl. Phys., Part 2* **1993**, *32*, L1577−L1580.
(32) Ban, S.; Maruno, S. *J. Biomed. Mater. Res.* **1998**, *42*, 387−395.
(33) Ban, S.; Hasegawa, J. *Biomaterials* **2002**, *23*, 2965−2972.
(34) Roeder, R. K.; Converse, G. L.; Leng, H.; Yue, W. *J. Am. Ceram. Soc.* **2006**, *89*, 2096−2104.
(35) Xie, R. Q.; Feng, Z. D.; Li, S. W.; Xu, B. B. *Cryst. Growth Des.* **2011**, *11*, 5206−5214.
(36) Kawasaki, T.; Niikura, M.; Kobayashi, Y. *J. Chromatogr.* **1990**, *515*, 125−148.
(37) LeGeros, R. Z., *Calcium Phosphates in Oral Biology and Medicine*; S. Karger: 1991.
(38) Gouzinis, A.; Tsapatsis, M. *Chem. Mater.* **1998**, *10*, 2497−2504.
(39) Lai, Z. P.; Bonilla, G.; Diaz, I.; Nery, J. G.; Sujaoti, K.; Amat, M. A.; Kokkoli, E.; Terasaki, O.; Thompson, R. W.; Tsapatsis, M.; Vlachos, D. G. *Science* **2003**, *300*, 456−460.
(40) Lin, J. C.; Yates, M. Z. *Chem. Mater.* **2006**, *18*, 4137−4141.
(41) van der Drift, A. *Philips Res. Rep.* **1967**, *22*, 267−288.
(42) Chen, C. L.; Li, J. Q.; Huang, Z. L.; Cheng, X. K.; Yu, J.; Wang, H.; Chi, R. A.; Hu, Y. H. *J. Cryst. Growth* **2011**, *327*, 154−160.